ROYAL SOCIETY
OF CHEMISTRY

Check for updates

An erythrocyte membrane-modified biomimetic synergistic nanosystem for cancer anti-vascular therapy and initial efficacy monitoring†

Jieying Zhang,[a] Fang Li,[a] Lili Su,[b] Qian Hu,[a] Jianfeng Li*[b] and Xingjun Zhu [iD] *[a]

Tumor vascular disruption has become a promising strategy for cancer therapy in recent decades. Nanocomposites loaded with therapeutic materials and drugs are expected to improve the accuracy of anti-vascular therapy and minimize side effects. However, how to prolong blood circulation of therapeutic nanocomposites for enhanced accumulation in tumor vasculature and how to monitor the initial efficacy of anti-vascular therapy for early evaluation of prognosis remain unsolved. Herein, a biomimetic nanosystem consisting of erythrocyte membrane modified nanocomposites (CMNCs) is developed for cooperation to achieve anti-vascular cancer therapy and initial efficacy monitoring. By utilizing poly(lactic-*co*-glycolic acid) (PLGA) as the interface material, functional nanomaterials and drug molecules are successfully integrated into CMNCs. The long circulation and immune escape features of the erythrocyte membrane facilitate CMNCs loaded with photothermal agents and chemodrugs to be delivered to the tumor region for anti-vascular treatment. Furthermore, the vascular damage-induced haemorrhage and the following coagulation process is labelled by near infrared emissive CMNCs to indicate the initial therapeutic efficacy of the treatment. This work not only points to a biomimetic strategy for conquering the challenges in anti-vascular cancer therapy, but also provides insights into the biological responses of erythrocyte membrane modified nanocomposites to exploit their biomedical applications.

1 Introduction

Tumor vasculature has become an interesting target for cancer therapy in the past decades, as it is closely related to nutrients and oxygen supply for the continuous growth of tumors.[1-4] For the disruption of tumor vasculature, vascular-disrupting agents (VDAs) including tubulin-binding agents, flavonoids and chemodrugs are developed to injure the endothelial cells and destroy the tumor vessels.[5-9] For example, doxorubicin (DOX), a chemotherapy drug, has also been reported for its contribution to vascular injury and enhancing platelet functions for coagulation, which exhibits toxicity in both tumor cells and tumor vessels, thus making up for the deficiency of infiltration in tumor margins in other VDAs.[10] In recent years, nanomaterials have

been utilized as VDA-carriers to reduce the off-target effect of VDAs that causes side effects in non-targeted tissues. Specific types of nanomaterials such as the ones with photothermal functions are also developed for destroying tumor vasculature *via* thermal ablation with a confined killing effect in the tumor region.[11-13] Nevertheless, there are still some challenges in cancer anti-vascular treatment. One is the optimization of blood circulation time of vascular disrupting drugs and nanomaterials to enhance their accumulation in the tumor vasculature. On the other hand, it is still difficult to monitor the initial effect of anti-vascular treatment, which provides the basis of treatment plan adjustment and the key signal for the prediction of prognosis.[14] Conventional methods for therapeutic effect evaluation such as the observation of tumor growth take a relatively long time period, which cannot reflect early vascular injury. Hence, it is crucial to develop a comprehensive strategy for prolonging blood circulation of vascular-disrupting agents and achieving initial efficacy monitoring to improve cancer anti-vascular treatment.

To address the challenges in cancer anti-vascular therapy, one possible strategy is to endow vascular-disrupting agents and nanomaterials with biomimetic properties so that the biological processes related to the treatment can be utilized to ameliorate their performance. Cell membranes, which play key roles in performing the physiological functions of cells, are

[a] *School of Physical Science and Technology, ShanghaiTech University, 393 Middle Huaxia Road, Shanghai, 201210, P. R. China.*
  E-mail: zhuxj1@shanghaitech.edu.cn
[b] *Gene Editing Center, School of Life Science and Technology, ShanghaiTech University, 393 Middle Huaxia Road, Shanghai, 201210, P. R. China.*
  E-mail: lijf1@shanghaitech.edu.cn

† Electronic supplementary information (ESI) available: X-Ray powder diffraction analysis, SDS-PAGE protein analysis, UV-Vis absorption spectroscopy, cytotoxicity essay, histological analysis and tumor growth observation. See DOI: https://doi.org/10.1039/d3tb00807j

ideal candidates for the modification of therapeutic agents and nanomaterials. Cell membrane-modified nanocomposites (CMNCs) can precisely inherit the surface characteristics and membrane-related signalling pathways of the source cells, which are developed for drug delivery and cancer therapy.[15–30] The erythrocyte membrane, namely the red blood cell (RBC) membrane, is the first and the most commonly used one for the establishment of CMNCs. Owing to the highly flexible structure of RBCs and the proteins residing on the membrane which mediate the self-recognition of homologous RBCs, it exhibits excellent long circulation and immune escape abilities *in vivo*, which are favourable for enhancing the accumulation of therapeutic agents in the tumor.[31–36] Besides, the RBC membrane is expected to be applied to target haemorrhage. During the coagulation initiated by activated platelets after vascular disruption-induced haemorrhage, integrin receptors on the RBC membrane interact with fibrinogen to form a specific binding, which leads to the recruitment and aggregation of RBCs in haemorrhage sites for hemostasis.[37] Haemorrhage induced by vascular injuries could activate a coagulation cascade, in which RBCs will be recruited, so it is reasonable to anticipate that the RBC membrane modified nanocomposites will label the coagulation site so that the timely evaluation of anti-vascular treatment can be realized. As a result, the RBC membrane-modified CMNCs emerge as an ideal platform for cancer anti-vascular theranostics.

Herein, we proposed a synergistic nanocomposite system consisting of the RBC membrane-modified CMNCs for the disruption of tumor vasculature and the monitoring of the initial anti-vascular efficacy (Fig. 1). A general method for the synthesis of CMNCs is developed in this work, in which poly(lactic-*co*-glycolic acid) (PLGA) has good cell membrane affinity.[32,38,39] PLGA is used as an interlayer to realize RBC membrane coating on hydrophobic nanoparticles and endows the nanocomposite with an additional function of drug loading. The CMNCs loaded with photothermal Cu_7S_4 nanoparticles and doxorubicin (CMNC-Cu-DOX) were employed to achieve vascular destruction in the tumor region. Damaged tumor vasculature induces haemorrhage and the following coagulation process can be labelled with RBC membrane coated CMNCs. By administering CMNCs containing lanthanide luminescent nanoparticles (CMNC-Ln) with near infrared emission at the second optical biological window (NIR-II), the coagulation caused by the vascular injury is visualized by optical bioimaging so that the initial effect of the anti-vascular treatment can be monitored (Fig. 1b).

2 Materials and methods

2.1 Materials

Poly(D,L-lactide-*co*-glycolide) (PLGA) (lactide : glycolide = 50 : 50, M_W = 7000–17 000) was provided by Evonik Industries AG. Poly(vinyl alcohol) (PVA, $M_W \sim$ 47 000) was purchased from Macklin Co., Ltd. Lanthanide oxides Y_2O_3 (99.999%), Lu_2O_3 (99.999%), Yb_2O_3 (99.999%), Nd_2O_3 (99.999%) and Er_2O_3 (99.999%) were purchased from Adamas Co., Ltd. Lanthanide chloride ($LnCl_3$) were prepared by dissolving Ln_2O_3 (Y_2O_3, Yb_2O_3,
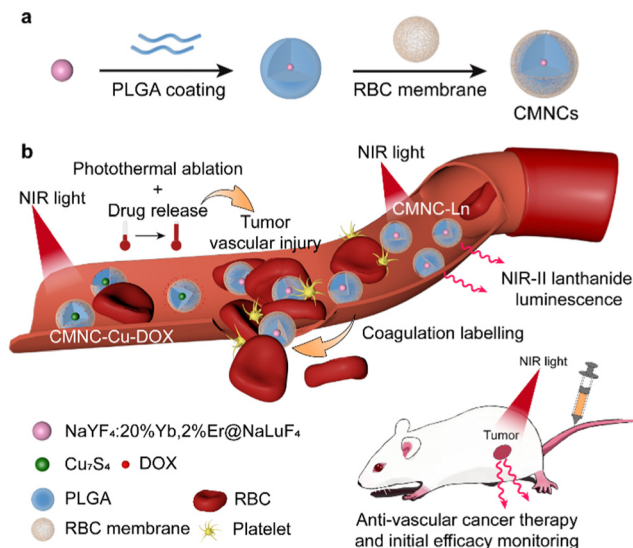

Fig. 1 (a) Synthetic procedures of the erythrocyte (RBC) membrane coated nanocomposites (CMNCs). (b) Schematic of the administration of CMNCs loaded with functional nanoparticles for anti-vascular cancer therapy and its initial efficacy monitoring. The first dose of CMNCs loaded with Cu_7S_4 nanoparticles and doxorubicin (CMNC-Cu-DOX) induced tumor vascular injuries due to the photothermal effect and drug release. The CMNCs loaded with $NaYF_4$:20%Yb,2%Er@$NaLuF_4$ nanoparticles with emission in the NIR-II region (CMNC-Ln) in the second dose participated in the coagulation process after vascular destruction attributed to the characteristic of the erythrocyte membrane surface to label the damaged region in the tumor vasculature. As a result, the efficacy of anti-vascular therapy can be monitored by the luminescence signal of CMNC-Ln.

Lu_2O_3, Er_2O_3, Nd_2O_3,) into hydrochloric acid (6 M) solution. The solution was then heated to evaporate water completely for the preparation of $LnCl_3$. 1-Octadecene (ODE, technical grade, 90%), oleic acid (OA, technical grade, 90%), and oleylamine (OLA, technical grade, 70%) were purchased from Sigma Aldrich Co., Ltd. Copper(II) chloride dihydrate ($CuCl_2·2H_2O$, 99.0%) was purchased from Greagent. Cyclohexane and ditertbutyl disulfide (97%) was purchased from Adamas Co., Ltd. Methanol, ethanol and NH_4F were purchased from Greagent Co., Ltd. Hydrofluoric acid, hexane, tetrahydrofuran (THF), and NaOH were purchased from Sinopharm Chemical Reagent Co., China.

2.2 Synthesis of $NaYF_4$:20%Yb,2%Er nanoparticles ($cNaLnF_4$)

$NaYF_4$:20%Yb,2%Er ($cNaLnF_4$) were synthesized under anhydrous and anaerobic conditions. A mixture of 0.78 mmol YCl_3, 0.2 mmol $YbCl_3$ and 0.02 mmol $ErCl_3$ was added to a three-neck flask with 6 mL OA and 15 mL ODE. The solution was placed under vacuum and heated to 120 °C to remove impurities. Then the solution was cooled to 60 °C, while 2.5 mmol NaOH and 4 mmol NH_4F dissolved in 4 mL methanol was added. After being heated to 90 °C for 30 min to evaporate methanol, the solution was swiftly heated to 305 °C under a nitrogen atmosphere and was kept at 305 °C for 1 h. After the solution was cooled to room temperature, the nanoparticles were washed twice with ethanol and eventually dispersed in cyclohexane.

This journal is © The Royal Society of Chemistry 2023

J. Mater. Chem. B, 2023, **11**, 7160–7168 | **7161**

2.3 Synthesis of core–shell NaYF$_4$:20%Yb,2%Er@NaLuF$_4$

NaYF$_4$:20%Yb,2%Er@NaLuF$_4$ (csNaLnF$_4$) were synthesized on the basis of cNaLnF$_4$. 0.5 mmol LuCl$_3$ was added to a three-neck flask with 6 mL OA and 12 mL ODE. The solution was vacuumed and heated to 120 °C to remove impurities. 0.5 mmol core sNaLnF$_4$ was redispersed in 3 mL ODE and added to the solution when it was cooled to 60 °C. 1.25 mmol NaOH and 2 mmol NH$_4$F dissolved in 4 mL methanol were added after the solution was kept at that temperature for 30 min. After being heated to 90 °C for 30 min to evaporate methanol, the solution was swiftly heated to 300 °C under a nitrogen atmosphere and was kept at 300 °C for 1 h. After the solution was cooled to room temperature, the nanoparticles were washed twice with ethanol and eventually dispersed in cyclohexane.

2.4 Synthesis of Cu$_7$S$_4$ nanoparticles

Cu$_7$S$_4$ nanoparticles were synthesized under anhydrous and anaerobic conditions. 0.5 mmol CuCl$_2$·2H$_2$O was added to a three-neck flask with 14.75 mL OLA. The solution was placed under vacuum at room temperature and 100 °C for 30 min respectively to remove vapor and impurities. Then the solution was heated to 200 °C under a nitrogen atmosphere and was kept at that temperature for 1 h. After the solution was cooled to 180 °C, 2.5 mL ditertbutyl disulfide was injected into the solution and the solution was kept at 180 °C for 40 min. The reaction was quenched by a nitrogen flow. After the solution was cooled to room temperature, Cu$_7$S$_4$ nanoparticles were washed twice with hexane and eventually dispersed in hexane.

2.5 Synthesis of the PLGA coated nanocomposite

csNaLnF$_4$ or Cu$_7$S$_4$ nanoparticles with a nanoparticle number of 6×10^{11} were mixed with 1.6 mg PLGA in THF to form a 200 μL mixture. Then the mixture was added dropwise into 1.5 mL of 0.1 wt% PVA aqueous solution with vigorous stirring. The solution was kept stirring at room temperature until THF was thoroughly evaporated. The solution was centrifuged at 9800g for 15 min to remove PVA to obtain PLGA coated csNaLnF$_4$ or Cu$_7$S$_4$ nanocomposites (csNaLnF$_4$@PLGA or Cu$_7$S$_4$@PLGA).

2.6 Doxorubicin loading in Cu$_7$S$_4$@PLGA

The as-synthesized Cu$_7$S$_4$@PLGA was resuspended in 600 μL of PBS and then 85 μL of doxorubicin (DOX) dissolved in PBS (2 mg mL^{-1}) was added and the mixture was stirred overnight. The solution was then centrifuged at 9800 g for 5 min to remove unloaded doxorubicin to obtain the doxorubicin loaded nanocomposite (Cu$_7$S$_4$@PLGA-DOX).

2.7 Extraction of the erythrocyte (RBC) membrane

Whole blood was collected from mice in phosphate buffer solution (PBS) with 0.25 mg mL^{-1} sodium heparin and 1 mM EDTA. Then the blood was washed no less than 3 times with PBS containing 1 mM EDTA to extract erythrocytes. The final volume of solution was doubled with PBS containing 1 mM EDTA. Starting from 250 μL of the solution containing erythrocytes, 950 μL of 0.2 mM EDTA in water and 50 μL 20× PBS were added sequentially and mixed well. The mixture was then centrifuged at 20 000 g to discard the supernatant. The last two steps should be repeated until the sediment turned white in color. Eventually, the sediment was resuspended in 250 μL of 0.2 mM EDTA in water. The content of the RBC membrane was expressed as the concentration of protein in the RBC membrane, and the protein concentration was quantified by the BCA assay to be about 13.50 mg mL^{-1}.

2.8 Synthesis of RBC membrane coated nanocomposites (CMNCs)

The as-prepared csNaLnF$_4$@PLGA or Cu$_7$S$_4$@PLGA-DOX was resuspended in 600 μL of deionized water (containing 1.33 mg mL^{-1} csNaLnF$_4$ or 0.25 mg mL^{-1} Cu$_7$S$_4$ nanoparticles). 150 μL of RBC membrane solution was added and mixed well. The mixture was then sonicated at hotspots of a bath sonicator for 3 min to perform coating. The mixture was centrifuged again after sonication at 4700g for 5 min to remove extra RBC membranes, and was eventually resuspended in deionized water to form pure aqueous solution of RBC membrane coated nanocomposites (CMNCs). CMNCs containing lanthanide luminescent nanoparticles were abbreviated as CMNC-Ln and the ones loaded with the Cu$_7$S$_4$ nanoparticles and DOX were abbreviated as CMNC-Cu-DOX.

2.9 Cell culture and cell viability assay

Human embryonic kidney (HEK) 293T cells were provided by the Shanghai Institute of Biochemistry and Cell Biology. The cells (5×10^6) were plated on a 6 cm dish and cultured with DMEM containing 10% fetal bovine serum at 37 °C and 5% CO$_2$ for 24 h. Cell viability was determined by the methyl thiazolyl tetrazolium (MTT) assay. The cells were transferred to a 96-well plate with 10^5 cells in each well and were cultured for at least 24 h and washed with phosphate buffer. Then the cells were incubated with CMNC-Ln at 37 °C and 5% CO$_2$ for another 48 h. After that, 20 μL MTT (5 mg mL^{-1} in phosphate buffer) was added to each well and incubated with cells at 37 °C and 5% CO$_2$ for 4 h. After discarding the solution, 150 μL DMSO was added to each well for measurements of optical density (OD$_{570}$) using a SpectraMax i3 multimode plate reader. The as-synthesized CMNCs were dispersed in PBS (pH 7.4) and stored at 4 °C.

2.10 Tumor xenograft

All animal procedures were performed under the guidance and approval of the Institutional Animal Care and Use Committee of ShanghaiTech University (Approval No. 20211115001). 4T1 cells were provided by Shanghai Institute of Biochemistry and Cell Biology. Cells (5×10^6) were planted on a 6 cm dish and cultured with RPMI-1640 medium (Adamas) containing 10% fetal bovine serum at 37 °C and 5% CO$_2$ for 24 h. The cells were washed and harvested with phosphate buffer, collected through centrifugation and eventually resuspended in RPMI-1640 medium without fetal bovine serum. The 6-week-old female Balb/c mice were injected subcutaneously with 4T1 cells (5×10^6 cells per mouse).

7162 | J. Mater. Chem. B, 2023, **11**, 7160–7168

This journal is © The Royal Society of Chemistry 2023

2.11 *In vivo* anti-vascular monitoring and cancer therapy

The mice were ready for antitumor treatment after the diameter of tumor reached 0.5 cm. CMNC-Cu-DOX dispersed in PBS was administered to mice through a tail vein injection (200 μL, with Cu_7S_4 nanoparticles at a concentration of 1.3 mg mL^{-1}). The tumor tissue was then irradiated by a continuous wave 808 nm laser for 30 min and whole-body thermal-imaging was performed using a thermal camera (FLIR E53). The mice were ready for anti-vascular monitoring *via* bioimaging after the antitumor treatment was applied. CMNC-Ln were dispersed in PBS and injected through the tail vein (200 μL, with NaLnF$_4$ nanoparticles at a concentration of 6.9 mg mL^{-1}) quickly after antitumor treatment. Whole-body optical bioimaging was performed under the excitation of a continuous wave 980 nm laser (50 mW cm^{-2}) at 2 h, 6 h, and 24 h after the injection of CMNC-Ln. A 1300 nm long-pass filter was used to exclude the excitation light. The mice were sacrificed soon after finishing the last imaging, and the tumor and the main organs (including the heart, liver, spleen, lungs, and kidneys) were extracted for *ex vivo* imaging. The bioimaging of the tumor and the main organs was performed under the same conditions stated above. For the long-term therapeutic effect evaluation, tumor bearing-mice were administrated with CMNC-Cu-DOX (with Cu_7S_4 nanoparticle at a concentration of 1.3 mg mL^{-1}) and irradiated by a continuous wave 808 nm laser (0.5 W cm^{-2}) for 30 min on Day 0 and Day 1. The tumor growth was measured for 15 days. The survival of mice was observed for 21 days. When the tumor diameter exceeded 1 cm, the end point of survival observation was reached and the mice were euthanized.

3 Results and discussion

3.1 Characterization and optimizations of RBC membrane coated nanocomposites (CMNCs)

RBC membrane coated nanocomposites (CMNCs) were composed of functional inorganic nanoparticles as the core, PLGA interlayer and RBC membrane as the outmost layer (Fig. 1a). To investigate the synthetic parameters of CMNCs, lanthanide sodium fluoride nanoparticles, which were widely used in biomedical applications, were chosen as the example in this work (Fig. 2a). Core–shell NaYF$_4$:20%Yb,2%Er@NaLuF$_4$ nanoparticles (csNaLnF$_4$) were prepared by the epitaxial growth of the NaLuF$_4$ layer on NaYF$_4$:20%Yb,2%Er nanoparticles (cNaLnF$_4$) *via* a solvothermal methods. Both cNaLnF$_4$ and csNaLnF$_4$ were monodispersed with uniform morphology, which had average diameters of 20.0 and 26.4 nm, respectively, as shown by transmission electron microscopy (TEM) (Fig. S1, ESI,† and Fig. 2b). Dynamic light scattering (DLS) analysis showed that csNaLnF$_4$ were well dispersed in the organic solvent such as tetrahydrofuran (THF) with dynamic diameters of 26.18 nm (Fig. 3a). X-Ray powder diffraction (XRD) analysis indicated that the as-prepared csNaLnF$_4$ had good crystallinity and are referred to as hexagonal phase NaYF$_4$ (PDF#16-0334) (Fig. S2a, ESI†). The surface of csNaLnF$_4$ was modified with long alkyl chain ligands such as oleic acid, which was confirmed by Fourier transform infrared (FTIR) spectroscopy since the
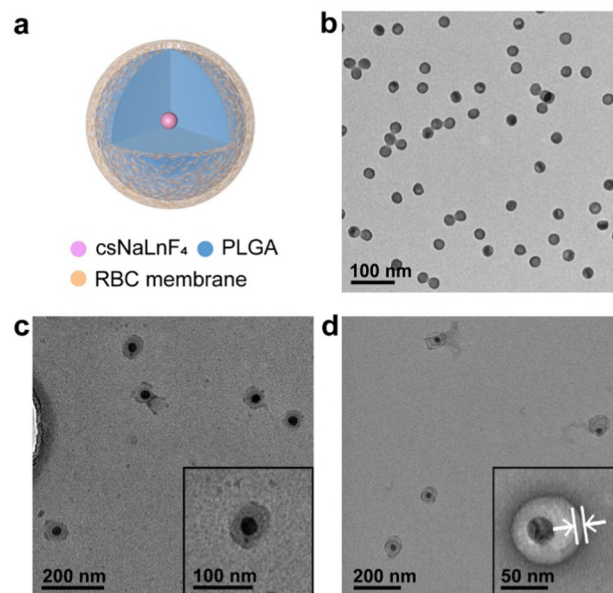
Fig. 2 (a) Schematic of the RBC membrane coated nanocomposites containing NaYF$_4$:Yb,Er@NaLuF$_4$ nanoparticles. Transmission electron microscopy (TEM) images of (b) NaYF$_4$:Yb,Er@NaLuF$_4$ nanoparticles (csNaLnF$_4$), (c) poly(lactic-*co*-glycolic acid) (PLGA) coated csNaLnF$_4$ (csNaLnF$_4$@PLGA) and (d) RBC membrane coated csNaLnF$_4$@PLGA (CMNC-Ln). The cell membrane is marked by white arrows in (d).
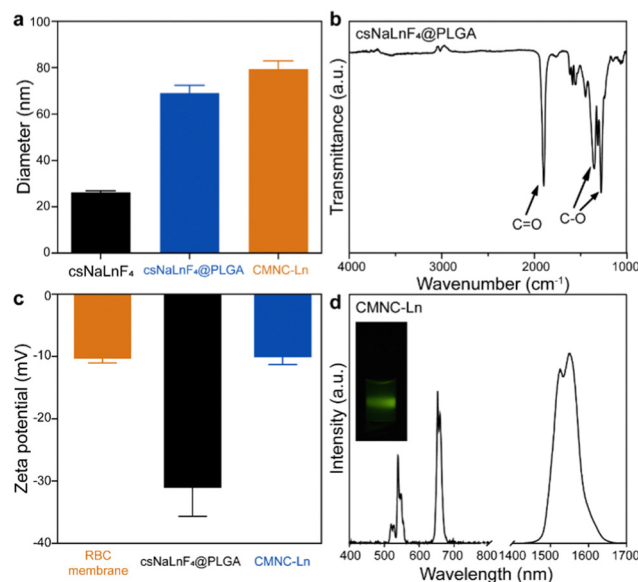
Fig. 3 (a) Size of nanocomposites measured by dynamic light scattering (DLS). Error bar stands for s.d. from $n = 3$ replicated samples. (b) Fourier transform infrared (FTIR) spectra of csNaLnF$_4$@PLGA. (c) Zeta potential of csNaLnF$_4$@PLGA, CMNC-Ln and RBC membrane. Error bar stands for s.d. from $n = 3$ replicated samples. (d) Upconversion and near infrared luminescence spectra of CMNC-Ln excited by a 980 nm laser with a 750 nm short-pass filter and a 1400 nm long-pass filter to exclude excitation, respectively.

transmission bands of C–H and C=O stretching vibrations could be identified (Fig. S2c, ESI†). As the widely reported inorganic nanoparticles with controllable size were usually

This journal is © The Royal Society of Chemistry 2023

J. Mater. Chem. B, 2023, **11**, 7160–7168 | **7163**

prepared by using non-polar reagents and ligands resulting in the hydrophobic nature of nanoparticles, the direct coating of the cell membrane on them would not be feasible. PLGA with acid modified terminations possesses hydrophobic moieties (*e.g.* a pendant methyl group on the alpha carbon of the lactic acid unit) to interact with nanoparticles and hydrophilic moieties (acid terminations) to achieve good dispersity in water, which is an ideal interface material for the phase transformation of the nanoparticles into an aqueous environment and the following cell membrane coating.

PLGA coated $csNaLnF_4$ ($csNaLnF_4@PLGA$) was fabricated by a co-precipitation method, in which $csNaLnF_4$ and PLGA were dispersed in THF and then the mixture was injected into aqueous solution. In the evaporation process, THF was gradually removed from the reaction system, which induced the assembly of PLGA outside the nanoparticles to form hydrophilic core–shell nanocomposites. The as-synthesized $csNaLnF_4@PLGA$ had spherical morphology with diameters of about 61.4 nm (Fig. 2c). The PLGA shell of $csNaLnF_4@PLGA$ was $\sim$11.3 nm in thickness. The strong absorption band at 1750 cm^{-1} assigned to C=O stretching vibrations was found in the FTIR spectrum of $csNaLnF_4@PLGA$, which also confirmed the successful modification of PLGA on $csNaLnF_4$ (Fig. 3b).

Red blood cell (RBC) membrane coating on $csNaLnF_4@PLGA$ was achieved *via* a sonication-induced assembling process. Based on previous work, the disruptive force induced by ultrasonic energy was supposed to initiate spontaneous coating of the cell membrane.[15] The semi-stability and charge asymmetry between cell membrane vesicles and nanoparticles were the key factors to determine the right-side-out coating of the cell membrane. With negative staining using uranyl acetate during TEM imaging, a coating layer with dark contrast could be seen on the surface of $csNaLnF_4@PLGA$ (Fig. 2d), which indicated the successful fabrication of cell membrane coated $csNaLnF_4@PLGA$ (abbreviated as CMNC-Ln). DLS data showed that the hydrodynamic diameter of CMNC-Ln increased to $\sim$79.3 nm compared to $csNaLnF_4@PLGA$ (69.0 nm) (Fig. 3a). Zeta-potential analysis revealed that CMNC-Ln became more positively charged (-10.16 mV) than $csNaLnF_4@PLGA$ (-31.20 mV) and the value was close to the one measured in the pure RBC membrane sample (-10.40 mV) (Fig. 3c), implying that the RBC membrane had been coated on the PLGA shell. Sodium dodecyl sulfate polyacrylamide gel electrophoresis (SDS-PAGE) was performed to demonstrate the reservation of RBC membrane proteins after coating. The results showed that CMNC-Ln had the same protein composition compared to the extracted RBC membrane indicating the successful cell membrane modification on the PLGA coated nanocomposite (Fig. S3, ESI†). The as-synthesized CMNC-Ln also showed consistency in data of DLS and zeta-potential analysis one week after synthesis, suggesting the ideal stability of the nanocomposite (Fig. S4, ESI†). After the RBC membrane coating, we tried to figure out whether the inorganic nanoparticle inside the CMNCs can still maintain their own properties. For instance, CMNC-Ln containing $NaYF_4$:Yb,Er@NaLuF$_4$ was excited by a 980 nm laser and its upconversion and down-shifting luminescence spectra were recorded. As shown in Fig. 3d, the upconversion emissions

at 540 and 660 nm which were generated from $^2H_{11/2}, ^4S_{3/2} \rightarrow ^4I_{15/2}$ and $^4F_{9/2} \rightarrow ^4I_{15/2}$ transitions and the NIR-II emission at 1550 nm derived from $^4I_{13/2} \rightarrow ^4I_{15/2}$ can be clearly identified, proving that the cell membrane coating would not affect the function of core nanoparticles for further applications.

3.2 Synthesis of CMNCs containing Cu_7S_4 nanoparticles

Next, we investigated the synthesis of CMNCs containing Cu_7S_4 nanoparticles and meanwhile validated the applicability of the cell membrane coating method on different types of inorganic nanoparticles (Fig. 4a). Cu_7S_4 nanoparticles with sphere-like morphologies were used as the core which had an average diameter of 26.2 nm as observed in the TEM image (Fig. 4b). The hydrodynamic size of Cu_7S_4 nanoparticles was measured to be 28.0 nm by DLS (Fig. S5a, ESI†). XRD analysis confirmed that the as-prepared Cu_7S_4 nanoparticles were identified as monoclinic Cu_7S_4 phase (PDF#23-0958) (Fig. S2b, ESI†). Ultraviolet-visible-near infrared (UV-Vis-NIR) absorption spectroscopy indicated that the Cu_7S_4 nanoparticles exhibited the near infrared (NIR)
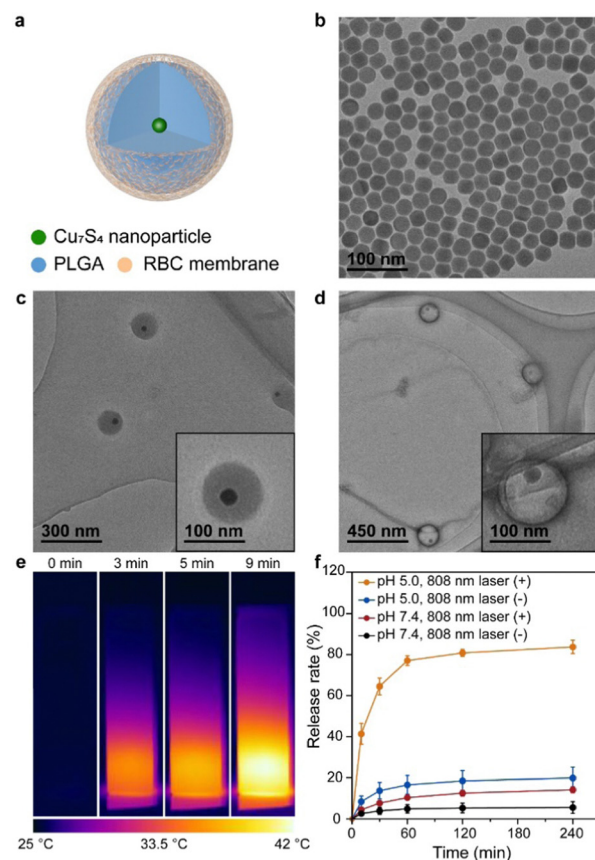

Fig. 4 (a) Schematic diagram of the RBC membrane coated nanocomposite with Cu_7S_4 nanoparticles and doxorubicin (CMNC-Cu-DOX). TEM image of (b) Cu_7S_4 nanoparticles. (c) PLGA coated Cu_7S_4 nanoparticles ($Cu_7S_4@PLGA$) and (d) RBC membrane coated $Cu_7S_4@PLGA$ (CMNC-Cu). (e) Infrared thermal images of CMNC-Cu excited by an 808 nm (0.5 W cm^{-2}) laser in aqueous solution for 9 min. (f) *In vitro* time-dependent doxorubicin release behavior of CMNC-Cu-DOX at pH 5.0 and 7.4 with or without a continuous wave 808 nm laser irradiation (0.5 W cm^{-2}). Error bar stands for s.d. from $n = 3$ replicated samples.

7164 | *J. Mater. Chem. B*, 2023, **11**, 7160–7168

This journal is © The Royal Society of Chemistry 2023

light-absorbing behavior starting from 700 nm (Fig. S5b, ESI†). Similar to csNaLnF$_4$, long alkyl chain ligands were modified on Cu$_7$S$_4$ nanoparticles, which were characterized by FTIR with the existence of the transmission bands of C–H, C=C and C–N stretching vibrations (Fig. S2d, ESI†). CMNCs containing Cu$_7$S$_4$ nanoparticles (denoted as CMNC-Cu, Fig. 4a) were synthesized by a similar protocol of CMNC-Ln. The average diameter of PLGA coated Cu$_7$S$_4$ nanoparticles (Cu$_7$S$_4$@PLGA) was 122.28 nm (Fig. 4c). After RBC membrane coating, the average diameter of CMNC-Cu was ∼145.2 nm as shown in the TEM image with negative staining (Fig. 4d). CMNC-Cu exhibited an excellent photothermal effect under the irradiation of an 808 nm laser (0.5 W cm^{-2}), of which the temperature of the PBS dispersion of CMNC-Cu increased from 25.2 °C to 41.8 °C in 9 minutes (Fig. 4e).

3.3 CMNCs for photothermal-controlled release of the vasculature disrupting agent

PLGA has been exploited as a drug carrier which could endow drug delivery function to the nanocomposite.[40–42] Considering the photothermal effect of CMNC-Cu excited by an 808 nm light source, it is expected to perform photothermal-controlled drug release under near infrared light irradiation. Doxorubicin (DOX) with vascular disrupting and anti-tumor effects was loaded in the PLGA layer of Cu$_7$S$_4$@PLGA by electrostatic interaction and then the RBC membrane was coated on the nanocomposite to form a drug delivery system (CMNC-Cu-DOX).[43] UV-Vis absorption spectroscopy revealed the successful loading of DOX since the absorption band of DOX centred at 485 nm appeared in CMNC-Cu-DOX sample compared to CMNC-Cu alone (Fig. S5c, ESI†). The loading ratio is calculated to be 11.9 µg DOX per milligram of CMNC-Cu. The drug release tests of CMNC-Cu-DOX were carried out in phosphate-buffered saline (PBS) at pH 5.0 and 7.4. In a neutral environment (pH = 7.4), the release of DOX was low (14.2%) under 808 nm irradiation. When the environment was changed to acidic conditions, there was a significant release of DOX (83.7%) from the nanocomposite and the release rate gradually reached a plateau after 1 h irradiation of a 808 nm laser, suggesting pH- and photothermal-dual responsive release behaviour of CMNC-Cu-DOX (Fig. 4f).

3.4 Demonstration of *in vivo* anti-vascular treatment and efficacy monitoring by CMNCs

Firstly, the cytotoxicity of CMNCs was evaluated in the human embryonic kidney (HEK) 293T cell line *via* the methyl thiazolyl tetrazolium (MTT) assay. Cells were incubated with media containing different concentrations of CMNC-Ln ranging from 0 to 400 µg mL^{-1} for 48 h. No significant difference was observed in cell growth when the incubating concentration of CMNC-Ln increased from 0 µg mL^{-1} to 400 µg mL^{-1}. The cell viabilities were all above 95.0%, indicating that CMNCs would not induce significant cytotoxicity (Fig. S6, ESI†).

Then the cytotoxicity of CMNC-Cu-DOX was also assessed for the demonstration of anti-tumor efficacy. Cells in the treatment group were initially incubated with media containing different concentrations of CMNC-Cu-DOX for 30 minutes with irradiation of a continuous wave 808 nm laser, while cells in the control group were not irradiated. The cells in both groups were incubated without irradiation for another 48 h. No significant difference was observed in cell growth when cells were not administered with CMNC-Cu-DOX. The cell viabilities were all above 83.3%, indicating that the irradiation of the NIR laser did not induce major damage in cells. However, with the increase of dose, the viability of cells significantly decreased to 42.7% and 18.3% when exposed to the laser (83.7% and 79.3% for the control group). The significant differences in cell viability between treatment and control groups indicated the therapeutic potential of CMNC-Cu-DOX in the tumor (Fig. S7, ESI†).

As photothermal treatment and DOX have been proven effective for vascular disruption, their combination was adopted for tumor anti-vascular therapy in this work. The treatment was carried out using CMNC-Cu-DOX with the NIR-responsive photothermal effect. Balb/c mice with orthotopic 4T1 breast cancer were used as an animal model. CMNCs dispersed in PBS were administered to mice through the tail vein (Fig. 5a). The tumor bearing mice were injected with CMNC-Cu-DOX first and then irradiated by a continuous wave 808 nm laser (0.5 W cm^{-2}) for 30 min to induce thermal ablation and chemotherapy on tumor vessels. Compared to the mice that were not injected with CMNC-Cu-DOX, the local temperature of tumors of mice injected with CMNC-Cu-DOX reached an average increment of 9.6 °C while the body temperature except the tumor region did not show an obvious elevation under infrared thermal imaging (Fig. 5b and c), and it took an average of 1.92 min to return to the initial temperature (Fig. S8, ESI†).

Tumor vessel injuries triggered the coagulation and CMNC-Ln modified with RBC membrane could be labelled on the damaged region to indicate vascular disruption efficacy. With the help of NIR-II emission of CMNC-Ln, the vascular disruption efficacy could be visualized by NIR-II optical bioimaging. Since the vessel disruptions and haemorrhage would continue during the photothermal process and the release of DOX,[11,44,45] the administration of CMNC-Ln to characterize the initial efficacy was launched after anti-vascular treatment to avoid the loss of CMNC-Ln through bleeding. The mice were injected with CMNC-Ln through the tail vein and NIR-II bioimaging was performed at 2 h, 6 h, and 24 h after dosing of CMNC-Ln, respectively, with a continuous wave 980 nm laser as excitation and a 1300 nm long-pass filter to exclude excitation light. The NIR-II luminescence signals can be detected in the main organs and tumor in the mice models *in vivo* during the period of 24 h after anti-vascular treatment. The accumulation of CMNC-Ln in the tumor increased gradually in the past 24 h and the mice with vascular disruption treatment exhibited higher NIR-II signal intensity than their counterpart without treatment (Fig. 5d and Fig. S9, ESI†). By normalizing the signal-to-noise ratio (SNR) of averaged luminescence intensity at the tumor site with the signals collected at 2 h after injection, it showed that the tumor mice with vascular disruption treatment had an averaged normalized SNR of 3.86 while the values of control groups with only irradiation, only CMNC-Cu-DOX administration and without any
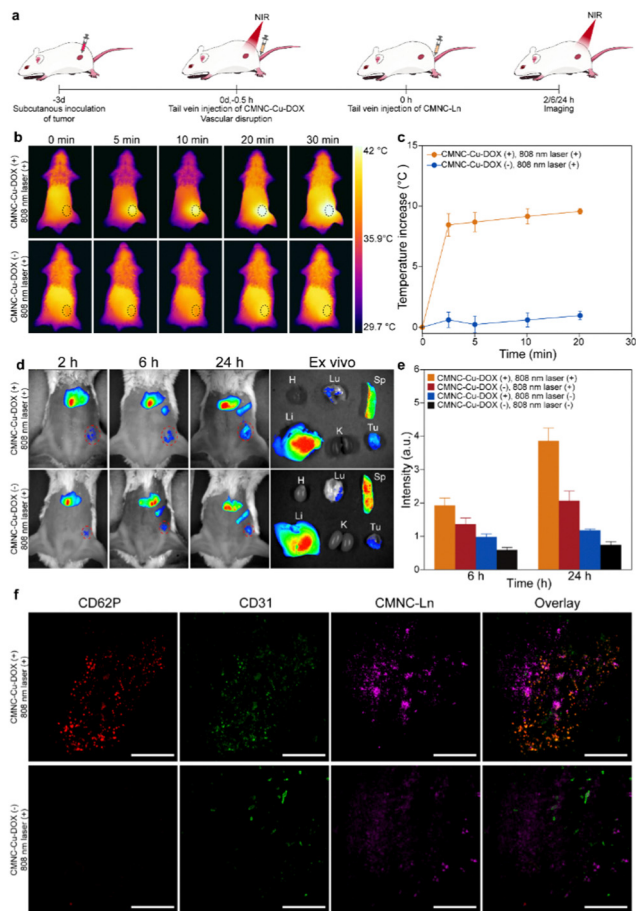
This journal is © The Royal Society of Chemistry 2023

J. Mater. Chem. B, 2023, **11**, 7160–7168 | **7165**

Fig. 5 Demonstration of *in vivo* anti-vascular treatment and efficacy monitoring. (a) Schematic illustration of initial treatment efficacy monitoring on tumor bearing mice. (b) Thermal images of a tumor-bearing mouse under an 808 nm laser irradiation. Tumor is marked with a black circle. (c) Elevation of temperature of mice with or without CMNC-Cu-DOX injection. Error bar stands for s.d. from $n = 3$ replicated samples. (d) Whole body NIR-II imaging of tumor-bearing mice and the main organs (heart (H), lungs (Lu), liver (Li), spleen (Sp), kidneys (K) and tumor (Tu)) with or without CMNC-Cu-DOX followed by 808 nm light irradiation. The tumor-bearing mice were injected with CMNC-Ln and the NIR-II luminescence was excited by a 980 nm laser with a 1300 nm long-pass filter. Tumor is marked with a red circle. (e) Normalized signal-to-noise ratio at the tumor site based on the signals at the time point of 2 h after injection in the anti-vascular treatment and control groups. Error bar stands for s.d. from $n = 3$ replicated samples. (f) The immunofluorescence images of tumor sections from mice with or without anti-vascular treatment. Scale bars were defined as 5 mm.

treatment were 2.07, 1.18 and 0.75, respectively (Fig. 5e). *Ex vivo* bioimaging of mice revealed that CMNC-Ln distributed mainly in the liver, spleen and tumor (Fig. 5d and Fig. S9, ESI†). Inductively coupled plasma atomic emission spectroscopy (ICP-AES) was used to quantitatively assess the amount of CMNC-Ln accumulated in tumor 24 h after vascular disruption treatment. The results showed that there was an elevated quantity of CMNC-Ln in tumors of mice with treatment (7.3%ID g^{-1}) compared to the control group without treatment (2.5%ID g^{-1}), proving that CMNC-Ln had been recruited to the treatment site and the feasibility to monitor the vascular injuries by CMNC-Ln (Fig. S10, ESI†).

To assess the initial anti-vascular effect in detail, the tumor tissue sections were stained with CD62P and CD31 antibodies. CD62P is the marker of platelets, while CD31 locates the vascular endothelial cells indicating the vasculature region. It showed that the vascular disruption treatment did cause damage to tumor vessels and triggered extensive coagulation in tumor tissues with platelets located in the vascular regions (Fig. 5f). The upconversion luminescence (UCL) of CMNC-Ln can be observed in the tumor section and the obvious aggregation of CMNC-Ln was observed in the tumor section from the treated mouse, while this could hardly be seen in tumors from mice without treatment (Fig. 5f). Furthermore, hematoxylin and eosin (H&E) staining of mice's organs and tumor tissue revealed that the malignant cells in tumor tissue with photothermal and chemodrug treatment showed shrinkage and fragmented nuclei upon the administration of CMNC-Cu-DOX, indicating that the nanocomposites had accumulated in the tumor site and the killing effect occurred (Fig. S11, ESI†). On the other hand, no significant damage appeared in the main organs (Fig. S11, ESI†). The results suggest that the CMNC system loaded with various functional nanoparticles could collaborate with each other to integrate vascular disruption treatment and efficacy monitoring, and the initial efficacy monitored on the treated mouse is expected to provide a prediction of favorable prognosis.

To validate the long-term therapeutic effect of CMNCs, tumor bearing mice were divided into four groups treated under different conditions. The group of mice administered with CMNC-Cu-DOX and irradiated by a continuous wave 808 nm laser (0.5 W cm^{-2}) for 30 min was set as the treatment group. The other two groups were treated with either CMNC-Cu-DOX or 808 nm laser irradiation, respectively. The mice without any treatment were set as the blank control. To assess the therapeutic effect, the sizes of tumors were measured during the treatment. In the treatment group, the tumors shrank significantly and crusts quickly formed on tumor sites four days after the treatment (Fig. 6a and Fig. S12, ESI†). The crusts eventually fell off 12 days later and the tumor was eliminated thoroughly and all four mice survived for 20 days, demonstrating the therapeutic effect of CMNC-Cu-DOX with the irradiation of NIR light (Fig. 6b and c). In contrast, tumors without any treatment grew rapidly and diameters of tumors soon reached 1 cm (Fig. 6c and Fig. S12, ESI†). CMNC-Cu-DOX or 808 nm laser irradiation alone did not induce obvious tumor growth suppression or survival rate enhancement compared to the treatment group (Fig. 6a–c and Fig. S12, ESI†). According to histological analysis after NIR irradiation, shrinkage and nuclei fragments of the cancer cells in the tumor could be observed in the treatment group compared to the ones in other three groups (Fig. 6d). The outcomes of the long-term tumor suppression were consistent with the predictions based on the initial efficacy monitoring using the NIR-II imaging function of CMNC-Ln, indicating that the RBC membrane modified CMNCs loaded with therapeutic and diagnostic nanomaterials not only achieved ideal therapeutic efficacy but also provided a strategy for prognosis evaluation at the early stage of treatment.
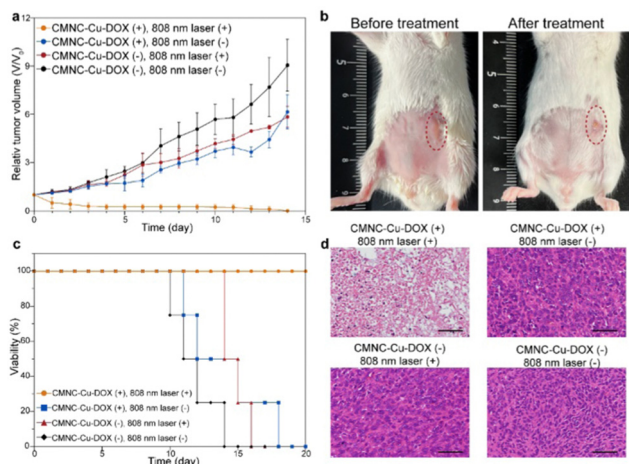
7166 | *J. Mater. Chem. B*, 2023, **11**, 7160–7168

This journal is © The Royal Society of Chemistry 2023

Fig. 6 Long term efficacy of *in vivo* anti-vascular treatment. (a) Growth of tumors with different treatments. Relative tumor volume was normalized based on the initial volume. Error bar stands for s.d. from $n = 4$ replicated samples. (b) Photos of tumor bearing mice before and after treatment. Tumor is marked with a red circle. (c) Survival curves of mice with different treatments. (d) Histological changes in the tumors of tumor-bearing mice with various treatments. The tumors were stained with hematoxylin and eosin (H&E), and scale bars were defined as 50 μm.

4 Conclusions

In conclusion, we have developed an RBC membrane modified nanocomposite-based strategy for cancer vascular disruption treatment and initial efficacy monitoring. Photothermal and lanthanide luminescence nanoparticles and small molecule drugs can be incorporated into the nanocomposite to achieve the corresponding therapeutic and diagnostic functions. Poly(lactic-*co*-glycolic acid) (PLGA) was utilized as an interface material to convert the nanoparticles' surface to hydrophilic for conquering the difficulty in cell membrane coating. By utilizing the long circulation and immune escape features of the RBC membrane, photothermal agents and drugs were delivered to the tumor region for vascular disruption treatment. Moreover, by taking advantage of the coagulation binding properties of the RBC membrane, the nanocomposites with NIR-II lanthanide luminescence are localized at vascular injuries, which is exploited to monitor the initial efficacy in the first 2 to 24 h after anti-vascular treatment. The initial efficacy monitoring based on NIR-II bioimaging matches well with the long-term observation of tumor growth suppression. This work provides insight into the biological functions of the RBC membrane to build cell mimicking nanocomposites for disease theranostics. At the same time, the cell membrane modification method proposed in this work is compatible with a variety of functional nanomaterials with hydrophobic surfaces and endows the nanocomposite with additional functions, such as drug loading and biological response, which greatly enhances the performance of nanomaterials for biomedical applications.

Data availability

The data that support the findings of this study are available in the ESI† of this article.

Author contributions

J. Z., J. F. and X. Z. conceived the project, analyzed the data, and wrote the original manuscript. J. F. and X. Z. supervised the project and acquired the financial support. J. Z., F. L., L. S., Q. H., J. F. and X. Z. designed the methodology, conducted the experiments and established the model for the study. The manuscript was written through contributions of all authors. All authors have given approval to the final version of the manuscript.

Conflicts of interest

There are no conflicts to declare.

Acknowledgements

References

1 J. Sawada, T. Urakami, F. Li, A. Urakami, W. Zhu, M. Fukuda, D. Y. Li, E. Ruoslahti and M. Komatsu, *Cancer Cell*, 2012, **22**, 235–249.

2 Z. Zhen, W. Tang, Y. J. Chuang, T. Todd, W. Zhang, X. Lin, G. Niu, G. Liu, L. Wang, Z. Pan, X. Chen and J. Xie, *ACS Nano*, 2014, **8**, 6004–6013.

3 M. Gil, M. Seshadri, M. P. Komorowski, S. I. Abrams and D. Kozbor, *Proc. Natl. Acad. Sci. U. S. A.*, 2013, **110**, E1291–E1300.

4 Y. X. Zhu, H. R. Jia, Y. Guo, X. Liu, N. Zhou, P. Liu and F. G. Wu, *Small*, 2021, **17**, e2100753.

5 M. M. Cooney, W. van Heeckeren, S. Bhakta, J. Ortiz and S. C. Remick, *Nat. Clin. Pract. Oncol.*, 2006, **3**, 682–692.

6 D. Banerjee, R. Harfouche and S. Sengupta, *Vasc. Cell*, 2011, **3**, 3.

7 W. Arap, R. Pasqualini and E. Ruoslahti, *Science*, 1998, **279**, 377–380.

8 D. W. Siemann and M. R. Horsman, *Cell Tissue Res.*, 2009, **335**, 241–248.

9 D. W. Siemann and W. Shi, *Int. J. Radiat. Oncol., Biol., Phys.*, 2004, **60**, 1233–1240.

10 L. Nguyen, T. Fifis, C. Malcontenti-Wilson, L. S. Chan, P. N. Costa, M. Nikfarjam, V. Muralidharan and C. Christophi, *BMC Cancer*, 2012, **12**, 522.

11 S. Hong, D. W. Zheng, C. Zhang, Q. X. Huang, S. X. Cheng and X. Z. Zhang, *Sci. Adv.*, 2020, **6**, eabb0020.

This journal is © The Royal Society of Chemistry 2023

J. Mater. Chem. B, 2023, **11**, 7160–7168 | **7167**

12 J. L. Paris, G. Villaverde, S. Gomez-Grana and M. Vallet-Regi, *Acta Biomater.*, 2020, **101**, 459–468.

13 X. Li, H. J. Yuan, X. M. Tian, J. Tang, L. F. Liu and F. Y. Liu, *Mater. Today Bio*, 2021, **12**, 100128.

14 B. Zhao, L. H. Schwartz and S. M. Larson, *J. Nucl. Med.*, 2009, **50**, 239–249.

15 R. H. Fang, A. V. Kroll, W. Gao and L. Zhang, *Adv. Mater.*, 2018, **30**, e1706759.

16 L. Rao, L.-L. Bu, Q.-F. Meng, B. Cai, W.-W. Deng, A. Li, K. Li, S.-S. Guo, W.-F. Zhang, W. Liu, Z.-J. Sun and X.-Z. Zhao, *Adv. Funct. Mater.*, 2017, **27**, 1604774.

17 S. Yaman, H. Ramachandramoorthy, G. Oter, D. Zhukova, T. Nguyen, M. K. Sabnani, J. A. Weidanz and K. T. Nguyen, *Front. Bioeng. Biotechnol.*, 2020, **8**, 943.

18 M. Gao, C. Liang, X. Song, Q. Chen, Q. Jin, C. Wang and Z. Liu, *Adv. Mater.*, 2017, **29**, 1701429.

19 R. H. Fang, C. M. Hu and L. Zhang, *Expert Opin. Biol. Ther.*, 2012, **12**, 385–389.

20 S. Aryal, C. M. Hu, R. H. Fang, D. Dehaini, C. Carpenter, D. E. Zhang and L. Zhang, *Nanomedicine*, 2013, **8**, 1271–1280.

21 J. A. Copp, R. H. Fang, B. T. Luk, C. M. Hu, W. Gao, K. Zhang and L. Zhang, *Proc. Natl. Acad. Sci. U. S. A.*, 2014, **111**, 13481–13486.

22 H. W. Chen, Z. S. Fang, Y. T. Chen, Y. I. Chen, B. Y. Yao, J. Y. Cheng, C. Y. Chien, Y. C. Chang and C. J. Hu, *ACS Appl. Mater. Interfaces*, 2017, **9**, 39953–39961.

23 A. Parodi, N. Quattrocchi, A. L. van de Ven, C. Chiappini, M. Evangelopoulos, J. O. Martinez, B. S. Brown, S. Z. Khaled, I. K. Yazdi, M. V. Enzo, L. Isenhart, M. Ferrari and E. Tasciotti, *Nat. Nanotechnol.*, 2013, **8**, 61–68.

24 W. He, J. Frueh, Z. Wu and Q. He, *Langmuir*, 2016, **32**, 3637–3644.

25 S. Thamphiwatana, P. Angsantikul, T. Escajadillo, Q. Zhang, J. Olson, B. T. Luk, S. Zhang, R. H. Fang, W. Gao, V. Nizet and L. Zhang, *Proc. Natl. Acad. Sci. U. S. A.*, 2017, **114**, 11488–11493.

26 Q. Hu, W. Sun, C. Qian, C. Wang, H. N. Bomba and Z. Gu, *Adv. Mater.*, 2015, **27**, 7043–7050.

27 Z. Chen, P. Zhao, Z. Luo, M. Zheng, H. Tian, P. Gong, G. Gao, H. Pan, L. Liu, A. Ma, H. Cui, Y. Ma and L. Cai, *ACS Nano*, 2016, **10**, 10049–10057.

28 A. V. Kroll, R. H. Fang, Y. Jiang, J. Zhou, X. Wei, C. L. Yu, J. Gao, B. T. Luk, D. Dehaini, W. Gao and L. Zhang, *Adv. Mater.*, 2017, **29**, 1703969.

29 Y. Wang, D. Wang, Y. Zhang, H. Xu, L. Shen, J. Cheng, X. Xu, H. Tan, X. Chen and J. Li, *Bioact. Mater.*, 2023, **22**, 239–253.

30 Y. Wang, X. Xu, X. Chen and J. Li, *Adv. Mater.*, 2022, **34**, e2107406.

31 W. Gao, C. M. Hu, R. H. Fang, B. T. Luk, J. Su and L. Zhang, *Adv. Mater.*, 2013, **25**, 3549–3553.

32 X. Zhang, P. Angsantikul, M. Ying, J. Zhuang, Q. Zhang, X. Wei, Y. Jiang, Y. Zhang, D. Dehaini, M. Chen, Y. Chen, W. Gao, R. H. Fang and L. Zhang, *Angew. Chem., Int. Ed.*, 2017, **56**, 14075–14079.

33 J. Su, H. Sun, Q. Meng, Q. Yin, S. Tang, P. Zhang, Y. Chen, Z. Zhang, H. Yu and Y. Li, *Adv. Funct. Mater.*, 2016, **26**, 1243–1252.

34 T. Liu, C. Shi, L. Duan, Z. Zhang, L. Luo, S. Goel, W. Cai and T. Chen, *J. Mater. Chem. B*, 2018, **6**, 4756–4764.

35 L. Wang, S. Chen, W. Pei, B. Huang and C. Niu, *J. Mater. Chem. B*, 2020, **8**, 4132–4142.

36 L. Rao, B. Cai, L. L. Bu, Q. Q. Liao, S. S. Guo, X. Z. Zhao, W. F. Dong and W. Liu, *ACS Nano*, 2017, **11**, 3496–3505.

37 R. I. Litvinov and J. W. Weisel, *ISBT Sci. Ser.*, 2017, **12**, 176–183.

38 C. M. Hu, R. H. Fang, K. C. Wang, B. T. Luk, S. Thamphiwatana, D. Dehaini, P. Nguyen, P. Angsantikul, C. H. Wen, A. V. Kroll, C. Carpenter, M. Ramesh, V. Qu, S. H. Patel, J. Zhu, W. Shi, F. M. Hofman, T. C. Chen, W. Gao, K. Zhang, S. Chien and L. Zhang, *Nature*, 2015, **526**, 118–121.

39 H. Sun, J. Su, Q. Meng, Q. Yin, L. Chen, W. Gu, P. Zhang, Z. Zhang, H. Yu, S. Wang and Y. Li, *Adv. Funct. Mater.*, 2016, **28**, 9581–9588.

40 Z. Zhang, S. Tongchusak, Y. Mizukami, Y. J. Kang, T. Ioji, M. Touma, B. Reinhold, D. B. Keskin, E. L. Reinherz and T. Sasada, *Biomaterials*, 2011, **32**, 3666–3678.

41 T. Govender, *J. Controlled Release*, 1999, **57**, 171–185.

42 S. Tan, T. Sasada, A. Bershteyn, K. Yang, T. Ioji and Z. Zhang, *Nanomedicine*, 2014, **9**, 635–647.

43 Q. Fu, P. Lv, Z. Chen, D. Ni, L. Zhang, H. Yue, Z. Yue, W. Wei and G. Ma, *Nanoscale*, 2015, **7**, 4020–4030.

44 H. Lv, R. Tan, J. Liao, Z. Hao, X. Yang, Y. Liu and Y. Xia, *Am. J. Physiol.: Heart Circ. Physiol.*, 2020, **319**, H133–H143.

45 P. Czupiel, V. Delplace and M. Shoichet, *Sci. Rep.*, 2020, **10**, 8726.

7168 | *J. Mater. Chem. B*, 2023, **11**, 7160–7168

This journal is © The Royal Society of Chemistry 2023